# Chapter 4

# A microscopic analysis of isospin effects on the onset of multifragmentation in light and heavy charged systems via Coulomb forces

## 4.1 Introduction

It is well known that the yield of intermediate mass fragments (IMFs) (produced in heavy-ion collisions at intermediate energies) is a good source to probe the dynamics of colliding nuclear matter [21, 22, 24, 92, 119, 121, 122, 125, 137, 138, 231, 240, 243, 244, 286]. As stated earlier, with the increase in the excitation energy, one may observe a rise and fall in the multiplicity of intermediate mass fragments [24, 92, 122, 125, 138, 231, 243, 286]. Also, it is worth mentioning that the critical energy point of the liquid-gas phase transition has been said to occur at intermediate energy in infinite nuclear matter and it may also be associated with the emission of fragments [92, 119, 121, 243, 245, 246, 266, 287, 288]. When charge (or mass) yields of fragments were fitted with exponential $\propto e^{-\lambda Z_f}$ ($e^{-\lambda A_f}$) or power law $\propto Z_f^{-\tau}$ ($A_f^{-\tau}$), a minima in $\lambda/\tau$ was reported with incident energy [92, 119, 121, 243]. Also, in this direction, additional scaling laws, for instance, Fisher scaling and Renormalization group (RG) scaling have been reported in the literature [266, 288] and it has been put forward that the physical parameters extracted from the fits strongly depend on the detailed shape assumed for the scaling function with the exception of parameters (like $\tau$ and others) which are consistent with the critical exponents of the

liquid-gas phase transition [4, 20, 266, 288]. This critical energy point is related with the onset of multifragmentation [243]. However, this interpretation about the critical energy point was disputed as some studies associated this dependence with colliding geometry as the mass yields were averaged over entire impact parameter [231, 289]. A study carried out by Porile *et al.* [289] for proton induced reactions was classic example of such dispute. Later on, charge (or mass) yields were parameterized by power law of the form $\propto Z_f^{-\tau}$ ($A_f^{-\tau}$) for the central collisions only and above behavior was still observed in many cases [92, 119, 121, 243]. At the same time, it was pointed out that such minima couldn't be achieved for highly charged systems [122]. Interestingly, studies do exist in the literature where the above minimum in the power law behavior was depicted to be an accidental phenomenon [178, 231].

The onset of multifragmentation and its connection to the nuclear liquid-gas phase transition has been reported both experimentally and theoretically. For example, Li *et al.* [121] studied the $Z_f$ - distribution of fragments obtained from the central collisions of $^{40}_{18}$Ar + $^{45}_{21}$Sc at beam energies ranging between 15 and 115 MeV/nucleon and after parameterizing the $Z_f$ - distributions with power law $\propto Z_f^{-\tau}$, a minimum in the value of critical exponent at a beam energy of $\approx 23.9\pm0.7$ MeV/A was observed. William *et al.* [122] performed study to understand fragment distributions for highly charged system using Statistical Multifragmentation Model (SMM) and reported the absence of above minimum in the critical exponent ($\tau$) when plotted against incident energy. A thorough survey of the literature also reveals that Quantum Molecular Dynamics (QMD) model [35, 290] approach has been reported to study the onset of multifragmentation [87, 243]. At the same time, recent interest of the community has shifted to isospin physics. The basic cause of this shift is the availability of radioactive ion beams. Accordingly, most of the theoretical models have also been upgraded to include isospin degree of freedom [186, 187, 189, 291] that gives greater insight about the reaction dynamics. Unfortunately, the studies of the charge (or mass) yields are very rare where isospin-dependent quantum molecular dynamics model is used [24, 158, 292]. On the other hand, many studies do exist in the literature where charge (or mass) yields have been studied for different input channels i.e., incident energies and colliding geometries [92, 119, 121, 122, 231, 243, 245]. However, no attention has been paid before to study the role of nuclear equation of state (NEOS) and its momentum dependence in the light of Coulomb forces on the onset of multifragmentaion in nearly symmetric and asymmetric reactions (taking light and

heavily charged systems) using Isospin-dependent Quantum Molecular Dynamics (IQMD) model [189]. Therefore, in this chapter, we will explore the effect of isospin degree of freedom via Coulomb forces on the onset of multifragmentation using both static and momentum-dependent interactions. This will help to probe the influence of Coulomb forces on critical energy point (i.e., the onset of multifragmentation) both for nearly symmetric and asymmetric collisions. Before moving to the results and discussions section, let us first discuss momentum-dependent interactions and their influence on the yield of fragments both in central and peripheral collisions for nearly symmetric and asymmetric reactions.

## 4.2 The momentum-dependent interactions

As discussed in Chapter 2, the parametrization of Skyrme interactions is an oversimplified prescription and does not take into account the exchange effects on nucleon-nucleon interaction (as $V^{Sky}$ scales to the single density-dependent parts [Eq. 2.26]). The exchange interactions create momentum dependence of the mean field. The interpretation of the momentum dependence of mean field is noticed from the proton-nucleus optical potential measured in the kinetic energy range from 10 MeV to 1 GeV [293]. Also, it is worth mentioning that along with density, momentum space is equally important in determining the fate of a reaction [35]. When one works within the framework of G-matrix (which is the solution of Bethe-Goldstone equation), the momentum dependence of the mean field comes in a natural way [250]. But to solve this equation numerically at each point (in the phase space) is a very complicated job and also the numerical utility of the G-matrix is very limited. [35]. Therefore, as a substitute, we use parameterized momentum-dependent potential which takes care of the momentum dependence in mean field potential. By fitting the experimental data on the real part of the optical potential, momentum-dependent interactions can be obtained.

The equation corresponding to the parameterized momentum-dependent potential is given by:

$$V_{ij}^{MDI} = t_4 \ell n^2[t_5(\mathbf{p}_i - \mathbf{p}_j)^2 + 1]\delta(\mathbf{r}_i - \mathbf{r}_j), \tag{4.1}$$

where, values of $t_4$ and $t_5$ are 1.57 MeV and $5\times10^{-4}$ MeV$^{-2}$, respectively. The final form of the momentum-dependent potential in terms of density is given as:

$$U^{MDI} = \delta \ell n^2[\epsilon(\rho/\rho_0)^{2/3} + 1]\rho/\rho_0. \tag{4.2}$$

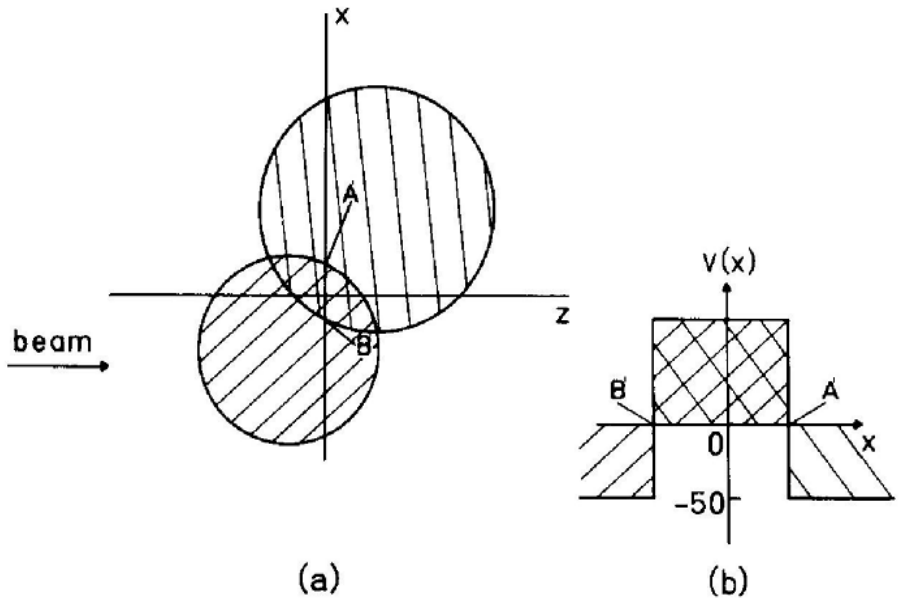


Figure 4.1: The transverse momentum caused by momentum-dependent forces. (a) The reaction in the beam-impact parameter plane. (b) The potential is along the X-axis. There is a strong repulsive and attractive potential in the overlap region and outside this region, respectively and therefore, the particles want to leave the overlap region by acquiring transverse momentum. "Reprinted from Physics Reports, **202**, J. Aichelin, Quantum molecular dynamics-A dynamical microscopic n-body approach to investigate fragment formation and the nuclear equation of state in heavy ion collisions, 233-360, Copyright (1991), with permission from Elsevier".

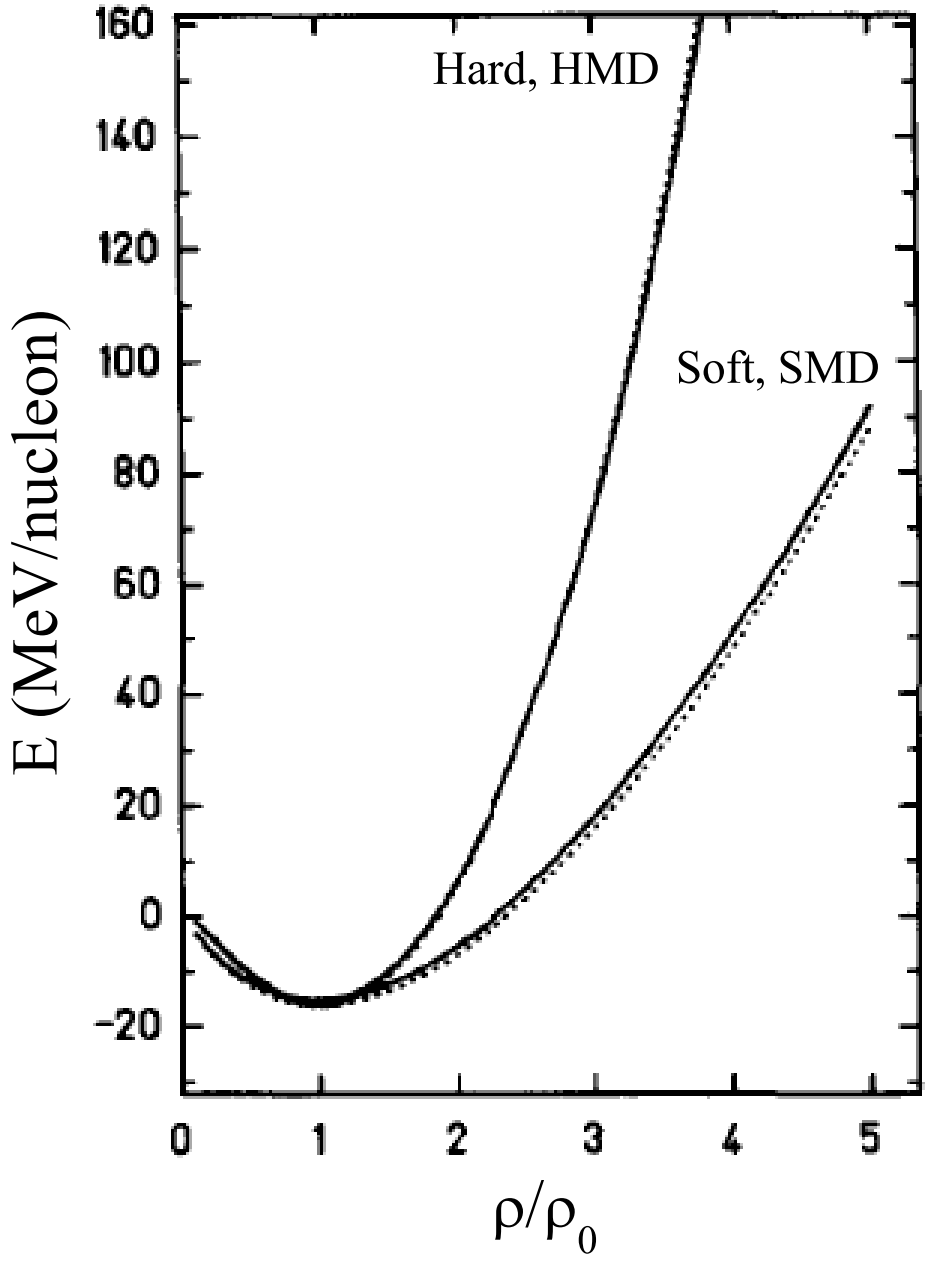


Figure 4.2: The density dependence of the energy per nucleon. The Soft, Hard, SMD, and HMD interactions are represented by dash-dot-dash, solid, dashed, and dash-double dotted lines, respectively. "Reprinted from Physics Reports, **202**, J. Aichelin, Quantum molecular dynamics-A dynamical microscopic n-body approach to investigate fragment formation and the nuclear equation of state in heavy ion collisions, 233-360, Copyright (1991), with permission from Elsevier".

Table 4.1: Parameters corresponding to the static and momentum-dependent potentials.

| K (MeV) | $\alpha$ (MeV) | $\beta$ (MeV) | $\gamma$ | $\delta$ (MeV) | $\varepsilon$ | EOS |
|---|---|---|---|---|---|---|
| 200 | -356 | 303 | 1.17 | - | - | Soft |
| 380 | -124 | 71 | 2.00 | - | - | Hard |
| 200 | -390 (-3189)$^{\dagger}$ | 320 (-3176)$^{\dagger}$ | 1.14 (1.011)$^{\dagger}$ | 1.57 | 21.54 | SMD |
| 380 | -130 (-63.13)$^{\dagger}$ | 59 (-49.42)$^{\dagger}$ | 2.09 (2.12)$^{\dagger}$ | 1.57 | 21.54 | HMD |

Again, local plus momentum-dependent potential can be parameterized in the form.

$$U = \alpha\left(\frac{\rho}{\rho_0}\right) + \beta\left(\frac{\rho}{\rho_0}\right)^{\gamma} + \delta\ell n^2[\epsilon(\rho/\rho_0)^{2/3} + 1]\rho/\rho_0. \tag{4.3}$$

One can use it to compute the corresponding density dependence of the compressional energy per nucleon. Thus, incorporating momentum-dependent interactions into the soft and hard equations of state give rise to soft momentum-dependent (SMD) and hard momentum-dependent (HMD) equations of state, respectively. The various parameters corresponding to different equations of state are listed in Table 4.1*. It is worth mentioning that a new parameterized form was later on put forward by Hartnack and Aichelin [226] based on the experimental analysis of Hama *et al.* [294]. Here, the bare interaction was folded with Gaussian wave function and results were fitted in QMD model with the help of the formula:

$$U_{12}(\mathbf{p}_1 - \mathbf{p}_2) = 0.0667 - \frac{0.0589}{(\mathbf{p}_1 - \mathbf{p}_2)^2 + 0.4837}. \tag{4.4}$$

It is worth mentioning that the momentum dependence of mean field plays an important role in deciding the dynamics of heavy-ion collisions. During the early phase (at the start) of the reaction, projectile and target are well separated and hence, the relative momentum of nucleons is very small, leading to insignificant contribution of the momentum-dependent interactions at this stage. But during the course of the reaction when projectile and target start overlapping as shown in Fig. 4.1(a), nucleons with large relative momentum come close to each other. The projectile nucleons face a very strong repulsion from target nucleons because of large relative momentum and vice-versa. But outside the overlap zone, nucleons in spectator zone are either from the projectile or target. The potential is

*Values labeled with '†' are based on the experimental data of Hama *et al.* [294] fitted by Hartnack and Aichelin [226].

still attractive in that region (see Fig. 4.1(b)) and the number of binary collisions reduces in this overlap region. In Fig. 4.2, the compressional energy per particle for static (soft and hard equations of state) and momentum-dependent interactions (SMD and HMD equations of state) as a function of density is shown. From the figure, it is clear that there is no difference between the static and momentum-dependent equation of state at normal nuclear matter density. But above the normal nuclear matter density, the difference between both equations of state goes on increasing. It has been reported in many previous studies that MDIs play crucial role in deciding the fate of reaction dynamics [295–298]. For instance, Aichelin *et al.* [295] reported in their study that MDIs have large influence on the $4\pi$ observables such as yields of Pions and Kaons and their sensitivity to momentum-dependent interactions. It was also found in Ref. [296] that the multiplicity of fragments gets enhanced for the highly mass asymmetric reactions once the momentum-dependent interactions are taken into account. Moreover, inclusion of MDIs in the mean field helps to reproduce the data, even with lower value of the compressibility [295, 297, 298]. Further, it was reported that in the presence of momentum-dependent interactions, sensitivity towards nucleon-nucleon cross-section diminishes [232]; whereas in other studies [299], the inclusion of MDIs enhances sensitivity of various observables such as nuclear stopping, free nucleons as well as the multiplicity of intermediate mass fragments (IMFs) towards the isospin dependence of the NN cross-section at high incident energies. Apart from the above forms of MDIs, different form such as GBD (i.e., momentum-dependent interaction used by Gale, Bertsch and Das Gupta) [298, 300] and MDY (momentum-dependent Yukawa interaction) [297] were also put forward in the literature.

### 4.2.1 Momentum-dependent interactions and the yield of fragments in nearly symmetric and asymmetric reactions

To address the question of the role of momentum dependence equation of state in nearly symmetric and asymmetric heavy-ion collisions, we simulated thousands of events for the reactions of $^{40}_{18}$Ar + $^{64}_{29}$Cu ($\eta = 0.23$), $^{40}_{18}$Ar + $^{108}_{47}$Ag ($\eta = 0.46$) and $^{40}_{18}$Ar + $^{197}_{79}$Au ($\eta = 0.66$) over a wide range of incident energy between 17 and 400 MeV/nucleon. First, we will shed light on the role of momentum-dependent interactions in central collisions and after that role of MDIs will be described for peripheral collisions in the dynamics of nearly symmetric and asymmetric reactions.

In Fig. 4.3, we display the size of heaviest fragment $<A_f^{max}>$ (top panels) and yields

of light charged particles LCPs (middle panels) and intermediate mass fragments IMFs ($3 \leq Z_f \leq 18$)(bottom panels) for the central collisions ($\hat{b}$ = 0 - 0.15) of $^{40}_{18}$Ar + $^{64}_{29}$Cu, $^{40}_{18}$Ar + $^{108}_{47}$Ag and $^{40}_{18}$Ar + $^{197}_{79}$Au as a function of beam energy using soft and soft momentum-dependent (SMD) equations of state. It is worth mentioning that the choice of soft equation of state is motivated from various studies which reported hadronic matter to be of softer nature [as reported in the Chapter 3]. From the figure, we notice that the size of $<A_f^{max}>$ decreases with increase in incident energy as expected because of violent collisions at higher beam energies. We also find that addition of momentum-dependent interactions lead to reduced $<A_f^{max}>$ because of additional breaking of correlations among nucleons. The difference in the size of $<A_f^{max}>$ is quite visible at lower beam energies. On the other hand, at very high beam energies, one sees almost same size of $<A_f^{max}>$ with soft as well as SMD equations of state. This is due to the fact that correlations at higher beam energies are already broken due to frequent binary collisions and therefore, additional momentum-dependent interactions do not play any significant role.

We also see that momentum-dependent interactions play enhanced role in reactions having higher mass asymmetry; size of $<A_f^{max}>$ reduces by 50% (at lower beam energies) in $^{40}_{18}$Ar + $^{197}_{79}$Au whereas, an approximate 35% reduction in $<A_f^{max}>$ is observed in the reaction of $^{40}_{18}$Ar + $^{64}_{29}$Cu. This happens because of comparatively less compression in highly asymmetric reaction of $^{40}_{18}$Ar + $^{197}_{79}$Au and thus momentum-dependent interactions break the correlations among interacting nucleons, which on the other hand, have been broken already to some extent due to significant overlapping in less asymmetric reaction of $^{40}_{18}$Ar + $^{64}_{29}$Cu. Following the trends in $<A_f^{max}>$, the corresponding multiplicities of LCPs and IMFs get enhanced when one use momentum-dependent interactions. From the figure, one also notices that for the reaction of $^{40}_{18}$Ar + $^{64}_{29}$Cu, SMD equation of state yields slightly lesser number of IMFs at higher energies above 100 MeV/nucleon. This interesting feature of IMFs production for less asymmetric system is because of the fact that in central collisions of nearly symmetric reactions, large destruction of initial nucleon-nucleon correlations already takes place (due to significant compression) and hence inclusion of momentum-dependent interactions further destroys the remaining correlations and leads to reduction in the multiplicity of IMFs and may result in enhanced yield of free nucleons and other lighter charged fragments. A rise and fall behavior in the IMFs multiplicity is also visible in highly asymmetric reactions of $^{40}_{18}$Ar + $^{197}_{79}$Au, as reported for symmetric reactions [125, 231, 286].

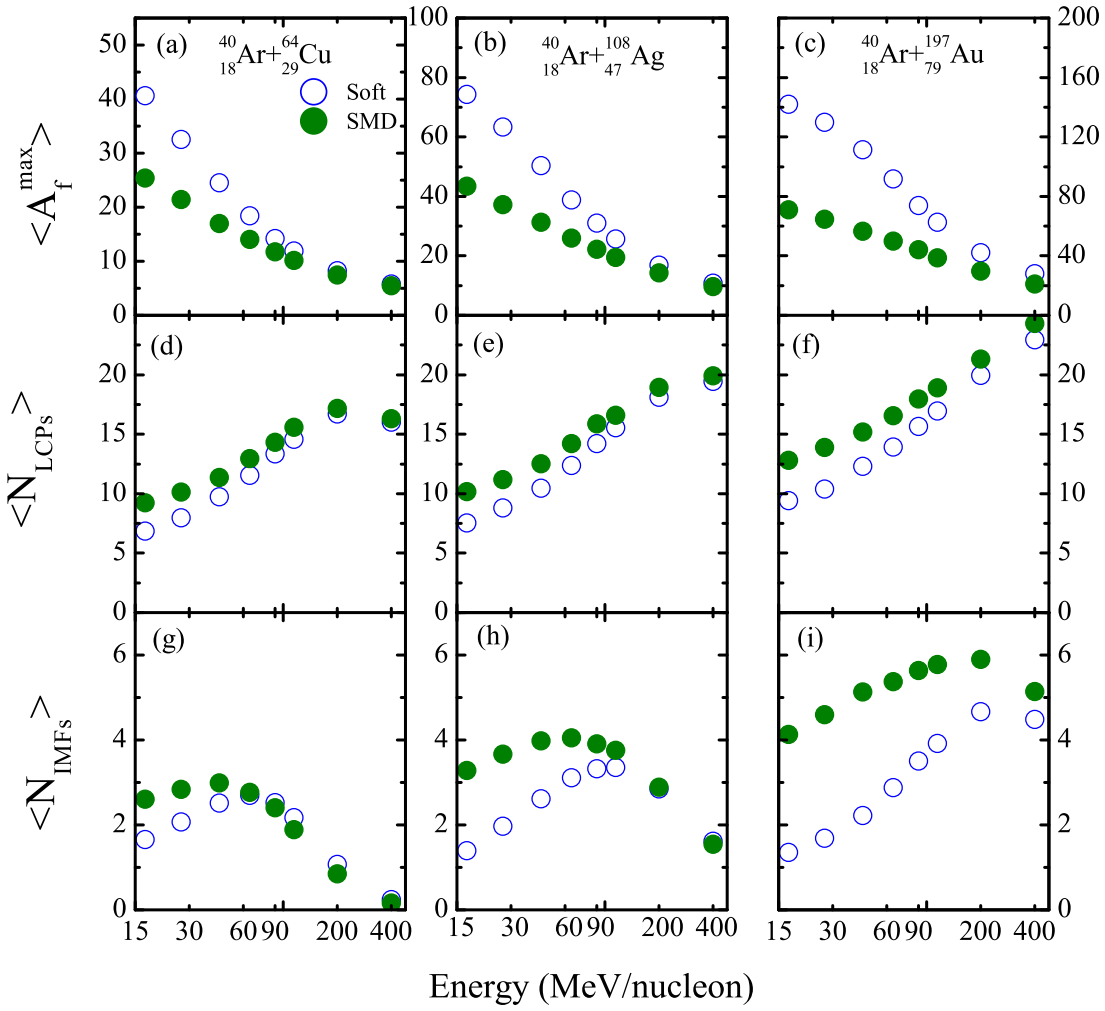


Figure 4.3: The size of heaviest fragment $<A_f^{max}>$ and multiplicities of light charged particles (LCPs) and intermediate mass fragments (IMFs) as a function of beam energy in the central collisions ($\widehat{b}$ = 0 - 0.15) of $^{40}_{18}$Ar + $^{64}_{29}$Cu, $^{40}_{18}$Ar + $^{108}_{47}$Ag and $^{40}_{18}$Ar + $^{197}_{79}$Au. Open (solid) symbols represent the results using soft (SMD) equation of state.

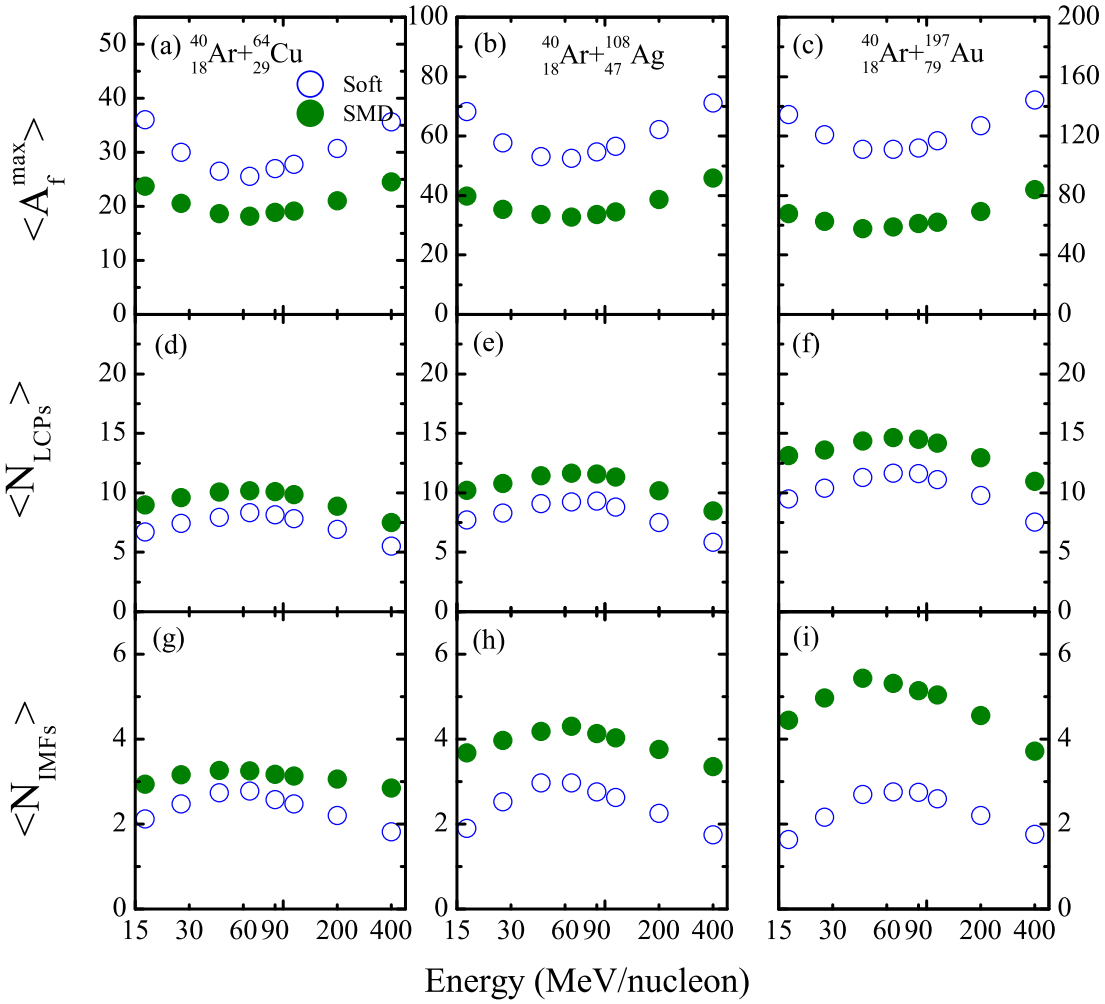


Figure 4.4: Same as Fig. 4.3, but at peripheral collisions ($\widehat{b} = 0.8$).

Next, we will study the effect of momentum-dependent interactions in the dynamics of asymmetric reactions at peripheral collisions. In Fig. 4.4 , we display the size of the heaviest fragment $<A_f^{max}>$ and multiplicities of LCPs and IMFs for the reactions mentioned above at peripheral collisions ($\hat{b} = 0.8$) using soft and soft momentum-dependent equations of state. The results are quite different than those observed for central colliding geometries (Fig. 4.3). In contrast to central collisions, where soft and soft momentum-dependent equations of state lead to same $<A_f^{max}>$ at higher beam energies, we observe a significant difference in the size of heaviest fragment (and thus various mass fragments's multiplicities) even at higher beam energies; with SMD equation of state yielding smaller $<A_f^{max}>$. This is because of the fact that the frequency of nucleon-nucleon collisions at peripheral geometry reduces significantly, leading to far less excited matter compared to central collisions where frequent nucleon-nucleon collisions disassemble the colliding nuclei.

Under these circumstances, momentum-dependent interactions play a significant role in breaking colliding nuclei into pieces of different sizes. Similar observations of enhanced role of momentum-dependent interactions at peripheral collisions have also been observed in the dynamics of transverse flow [295]. We also notice that the size of $<A_f^{max}>$ first decreases with beam energy, reaches a minimum and then a further increase is observed at very high beam energies contrary, to a monotonic decrease as noted in central collisions. This behavior is observed for all reactions independent of their mass asymmetry even at higher energies. A bigger $<A_f^{max}>$ at higher beam energies in peripheral collisions is because of less excited matter where projectile and target don't have enough time to interact (because of higher beam energy), only few nucleons's exchange will take place and size of $<A_f^{max}>$ is close to that of target mass. For example, $<A_f^{max}> = 60$ (160) in the reaction of $^{40}_{18}$Ar + $^{64}_{29}$Cu ($^{40}_{18}$Ar + $^{197}_{79}$Au) at 400 MeV/nucleon. This unusual behavior of $<A_f^{max}>$ at peripheral collisions of asymmetric reactions is also reflected in the multiplicities of light charged particles where a rise and fall is observed, contrary, to the central ones (monotonic rise is observed). The significant role of momentum-dependent interactions even at higher incident energies is because of the reduced compression at these geometries. The additional destruction of initial correlations happens due to inclusion of momentum-dependent interactions. As stated earlier, one looks for the onset of multifragmentation i.e., critical energy point for central collisions only, therefore, for further calculations, we will only take central colliding geometry. Hence, as noted in Figs.

4.3 and 4.4, MDIs affect the yield of fragments, therefore, we are interested here to find the effect of momentum-dependent interactions on the onset of multifragmentation (an important concept in nuclear physics) with and without the companionship of Coulomb forces.

## 4.3 Coulomb forces: an introduction

As already discussed in Chapter 2, isospin effects are incorporated via symmetry potential (to achieve correct distribution of protons and neutrons in the nucleus) and Coulomb forces between the projectile and target protons. Chragi and Gupta [301] reported that in the presence of Coulomb forces, there occurs a deviation in the trajectory of the projectile as shown in Fig. 4.5. In intermediate energy heavy-ion collisions, Coulomb interactions play significant role in various phenomena like multifragmentation, collective flow and nuclear stopping etc. The dominance of the Coulomb forces in these phenomena is because of its repulsive nature and effects are said to be more pronounced in the presence of symmetry energy [302]. Many studies do exist in the literature where isospin effects in terms of Coulomb interactions have been reported on various observables [301–305]. For example, Liu *et al.* [302] studied the isospin effect of Coulomb interactions on the momentum dissipation (or nuclear stopping) in intermediate energy heavy-ion collisions and revealed that the Coulomb interaction is preferable to study the isospin effect of in-medium nucleon-nucleon cross-section on the "R" and "$Q_{ZZ}$" (see Chapter 1 for the explanation of these variables) and to reduce the isospin effect of symmetry potential. Also, it has been reported in many studies [272, 303–306] that both Coulomb interactions as well as binary collisions affect the dynamics involving heavier colliding nuclei. In the absence of Coulomb forces, transverse flow decreases [284, 303, 304, 307]. Very recently, Puri and collaborators [276] studied the effect of Coulomb interactions on the energy of vanishing flow in the super-heavy mass region and interestingly, reported significant deviations from the power law mass dependence (for the energy of vanishing flow) in super-heavy nuclei when compared with stable systems, thus, marked the importance of Coulomb forces in the super-heavy systems.

Hence, as discussed above, both Coulomb forces and momentum-dependent interactions influence the dynamics of heavy-ion collisions and therefore, it will be interesting to see the effect of Coulomb forces on the onset of multifragmentation when momentum-

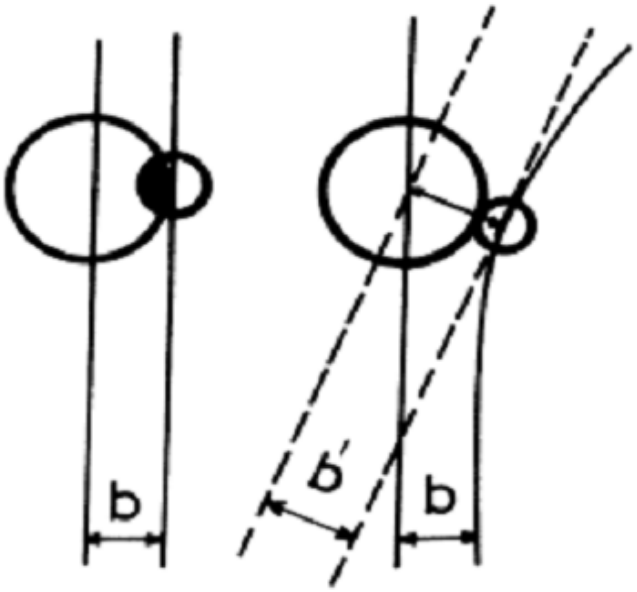


Figure 4.5: A comparison of the projectile trajectory with (right side) and without (left side) Coulomb field. "Reprinted from Physical Review C, **41**, S. K. Charagi and S. K. Gupta, Coulomb-modified Glauber model description of heavy-ion reaction cross sections, 1610, Copyright (1991), with permission from APS".

dependent interactions are also included in the propagation.

## 4.4 Results and discussions for the onset of multifragmentation

In order to study the relative role of static and momentum-dependent potential as well as Coulomb forces on charge yields, we generated several thousand events of the reactions of $^{40}_{18}$Ar + $^{45}_{21}$Sc (light charged system) and $^{84}_{36}$Kr + $^{197}_{79}$Au (heavily charged system) at different incident energies ranging between 15 and 400 MeV/nucleon using the static (soft) as well as soft momentum-dependent (SMD) equations of state with 20% reduced energy-dependent nucleon-nucleon cross-section i.e, $\sigma_{NN} = 0.8\sigma_{NN}^{free}$. Note that this reduction (20%) in the cross-section has also been taken in our previous study [24] (see Chapter 3) and is guided by various previous studies (as reported in Chapter 3). Also, the choice of soft and soft momentum-dependent equations of state for the current study is supported by earlier studies [24, 300, 308–313]. Here, also the reactions are simulated till 300 fm/c .

All the reactions are simulated for central colliding geometry ($\hat{b}$=0-0.25) only (guided from Refs. [24, 122, 138]). Thus, we will study the onset of multifragmentation in the presence (absence) of Coulomb forces for static (soft) and soft momentum-dependent (SMD) interactions by dividing the present study for light and heavily charged systems. First, we will focus on light charged system i.e., $^{40}_{18}$Ar + $^{45}_{21}$Sc

### 4.4.1 Onset of multifragmentation in light charged system

In Fig. 4.6, we display the calculated charge distributions for the reactions of $^{40}_{18}$Ar + $^{45}_{21}$Sc using soft as well as soft with momentum-dependent interactions at different bombarding energies (ranging between 15 and 115 MeV/nucleon). Open (solid) circles represent the calculations with soft (SMD) equation of state. Clearly, the charge distributions become steeper with increasing beam energy in both cases reflecting the violence of the collisions. These findings are in accordance with those reported in Refs. [24, 119, 121, 122]. We fit these charge distributions with power law ($\propto Z_f^{-\tau}$) for intermediate mass fragments ($3 \leq Z_f \leq 12$). The extracted values of the factor $\tau$ are plotted as a function of incident energy in Fig. 4.7 for soft as well as for SMD equations of state. Note that the values of $\tau$ for both the equations of state increase with incident energy reflecting the steepening of the charge distributions. Here, we do not observe any minima in the extracted values of $\tau$

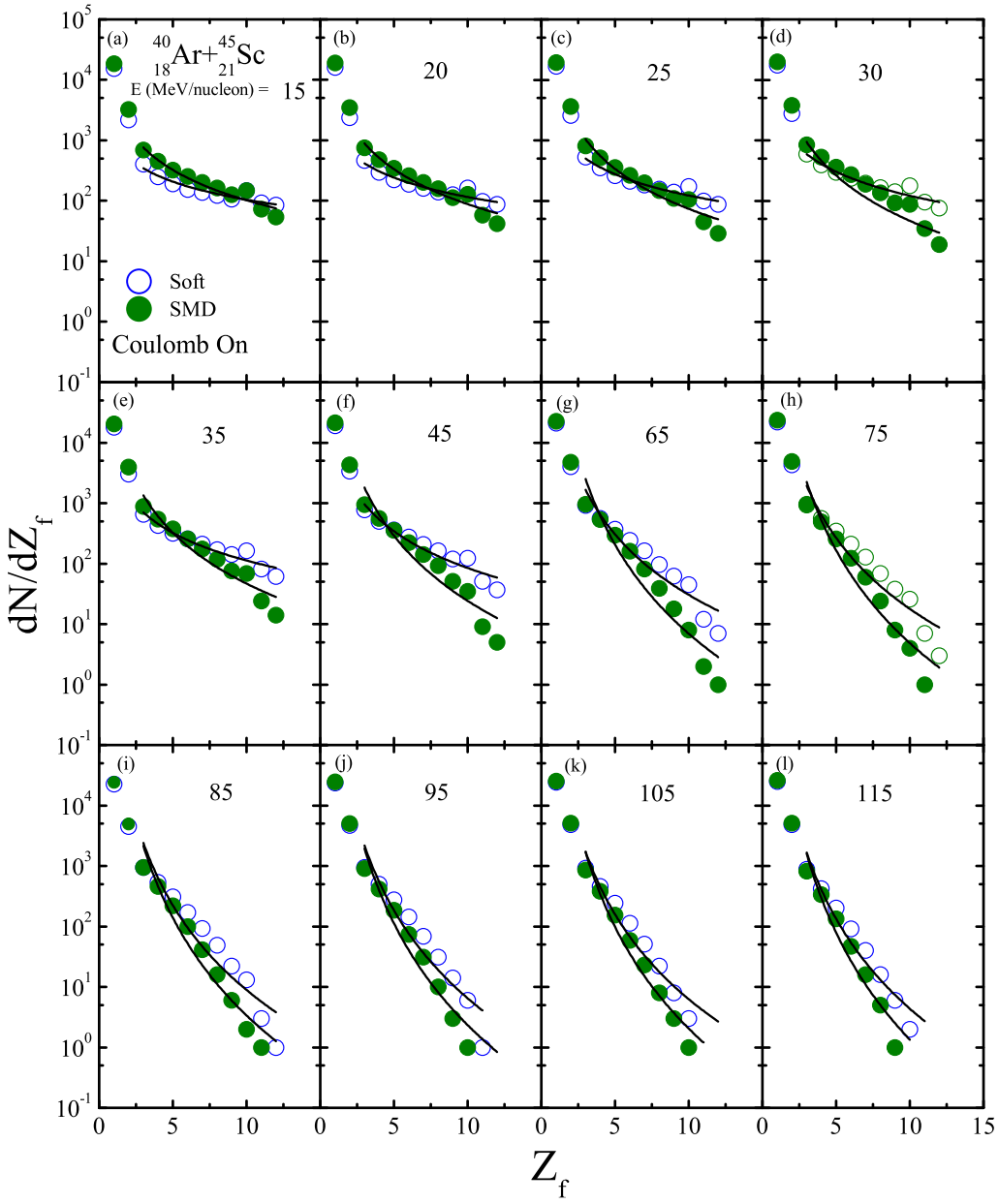


Figure 4.6: The charge distributions of the central collisions of $^{40}_{18}$Ar + $^{45}_{21}$Sc at beam energies between 15 and 115 MeV/nucleon. Open (solid) circles correspond to present calculations using soft (SMD) equation of state in the presence of Coulomb forces. The solid lines represent power law fits over intermediate mass fragments ($3 \leq Z_f \leq 12$).

when plotted against incident energy, rather a flat behavior of the parameter $\tau$ is observed for the soft equation of state at small incident energies ($<$ 20 MeV/A). This leads to the conclusion that the onset of the multifragmentation occurs at incident energies less than 15 MeV/nucleon for light charged colliding system of $^{40}_{18}$Ar + $^{45}_{21}$Sc. This may be due to the reason that by incorporating isospin degree of freedom, the Coulomb potential dominates (due to repulsive nature) and hence shifts the onset of multifragmention towards lower beam energies. Also, it is clear from Fig. 4.7 that the flat behavior of $\tau$ is not visible for SMD equation of state because by taking momentum-dependent interactions for nearly symmetric systems lead to more repulsions and thus, steepening of the charge distributions increases sharply even at lower incident energies for nearly symmetric collisions. Further, as mentioned above, Coulomb forces can affect the calculated charge distributions as well as the onset of multifragmentation, so, one is interested to see the influence of Coulomb forces on the charge yields as well as on parameter $\tau$.

In Fig. 4.8, we display the charge distributions for the above cases in the absence of Coulomb forces for central collisions of $^{40}_{18}$Ar + $^{45}_{21}$Sc. The charge distributions for the intermediate mass fragments are also fitted with power law $\propto Z_f^{-\tau}$ and the extracted $\tau$ values are plotted in Fig. 4.9.

Interestingly, the effect of Coulomb forces is visible even for the light charged system like $^{40}_{18}$Ar + $^{45}_{21}$Sc. The steepening of charge distributions in the absence of Coulomb forces gets slow down compared to the calculations with Coulomb forces. One also notices a little dip in the extracted values of $\tau$ for soft equation of state. The extracted $\tau$ values are fitted with fourth order polynomial fit to find the critical energy point. The minimum occurs at energy of $\simeq$ 22.07 $\pm$ 0.5 MeV/nucleon. Further, our calculations in the absence of Coulomb forces are consistent with those reported in Ref. [121].

To improve the accuracy of the critical energy point, we also fit the charge distributions ($3 \leq Z_f \leq 12$) in the absence of Coulomb forces with exponential fits of the form $\propto e^{-\lambda Z_f}$ as shown in Fig. 4.10 and the extracted $\lambda$ values are plotted against incident energy in Fig. 4.11. To obtain the critical energy point, we again fit the $\lambda$ values with fourth order polynomial fit and find that the critical energy point is obtained at $\simeq$ 22.07 $\pm$ 0.5 MeV/nucleon and is completely consistent with the one obtained by using power law fits. Here, the striking point is that the momentum-dependent interactions lead to the disappearance of the critical energy point and imparts its dominance even in the absence of Coulomb forces for light charged colliding systems. This creates curiosity to check the

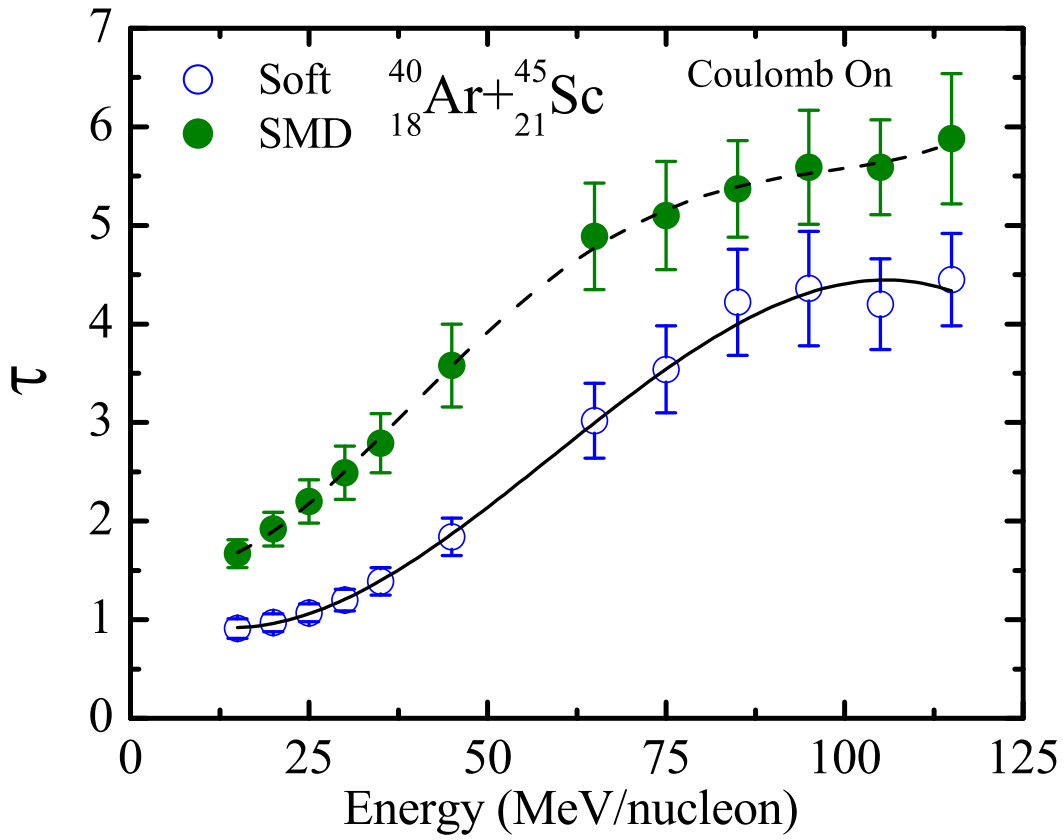


Figure 4.7: Extracted values of parameter $\tau$ obtained from the power law fits of intermediate mass fragments as done in Fig. 4.6. Symbols have the same meaning as in Fig. 4.6. Solid and dashed lines represent fourth order polynomial fits of $\tau$ values obtained using soft and SMD equations of state, respectively.

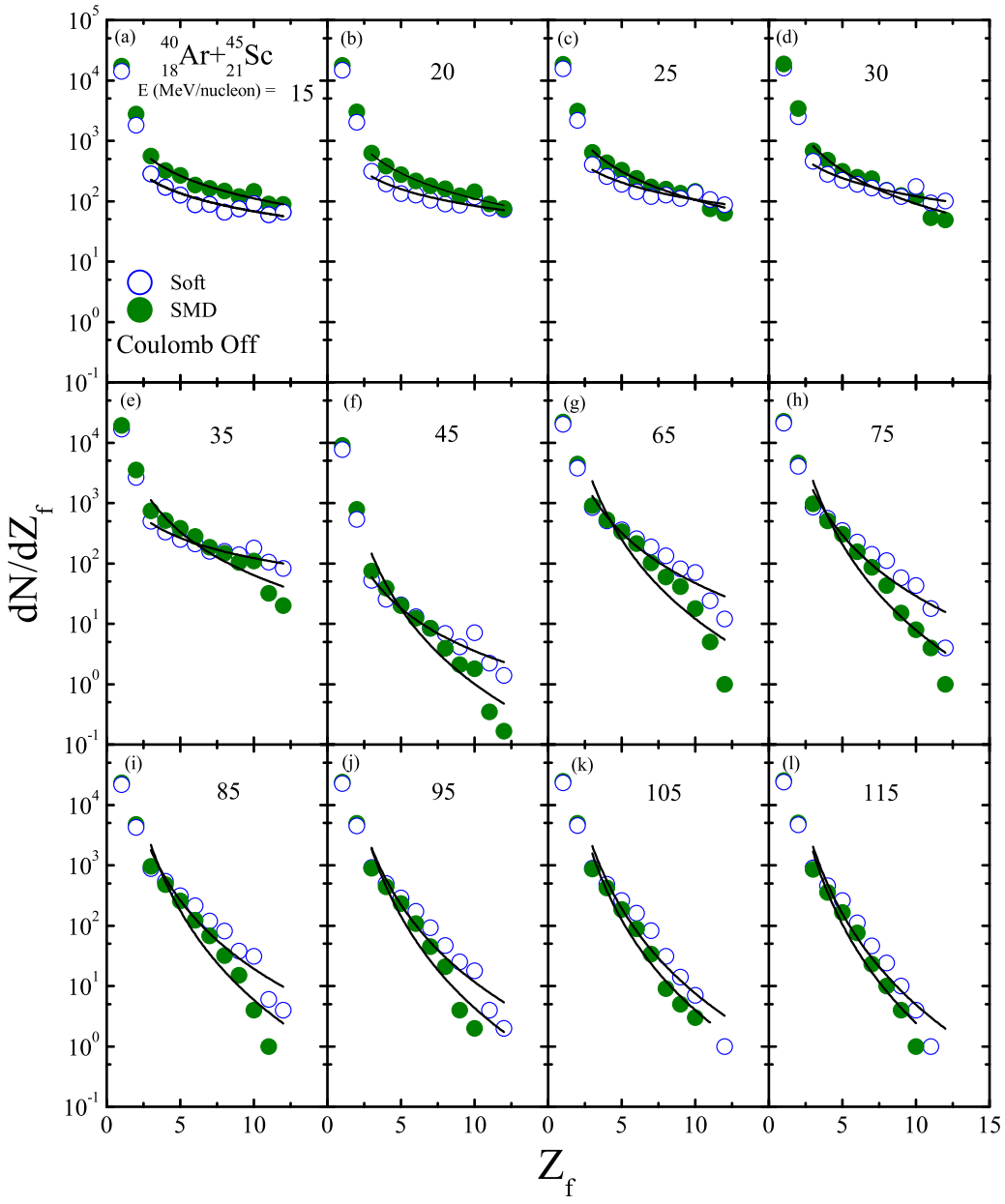


Figure 4.8: Same as Fig. 4.6, but in the absence of Coulomb forces.

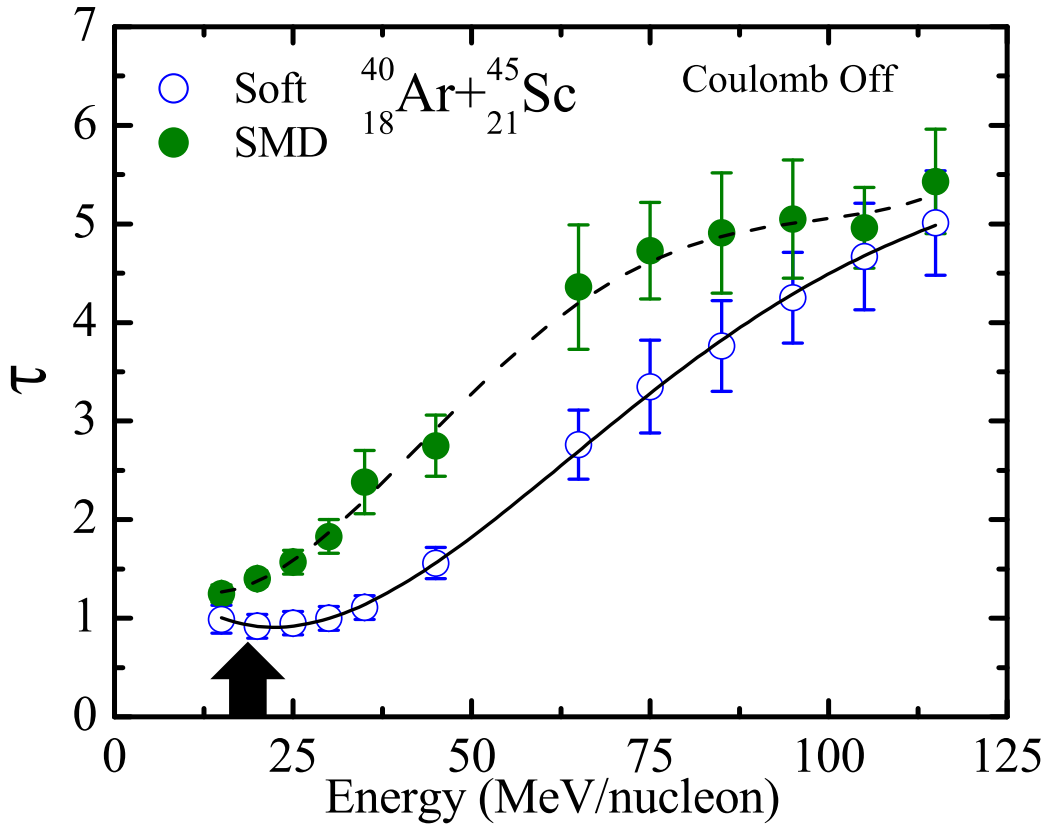


Figure 4.9: Same as Fig. 4.7, but in the absence of Coulomb forces. Here, solid arrow corresponds to the minimum in the extracted values of $\tau$ for soft equation of state.

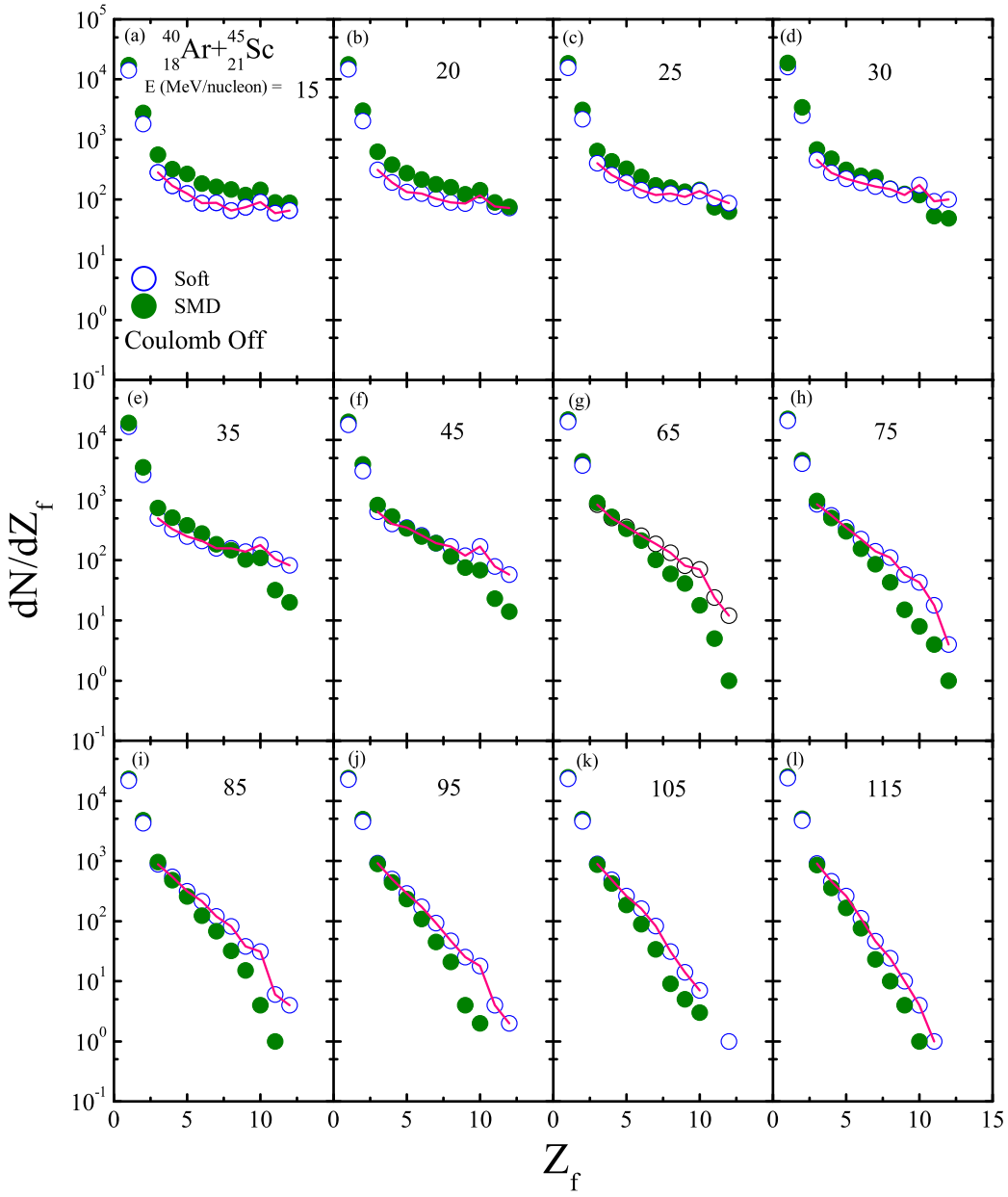


Figure 4.10: The charge distributions of the central collisions of $^{40}_{18}$Ar + $^{45}_{21}$Sc at beam energies between 15 and 115 MeV/nucleon. Open (solid) circles correspond to present calculations using soft (SMD) equations of state in the presence of Coulomb forces. The solid lines represent exponential fits over intermediate mass fragments ($3 \leq Z_f \leq 12$).

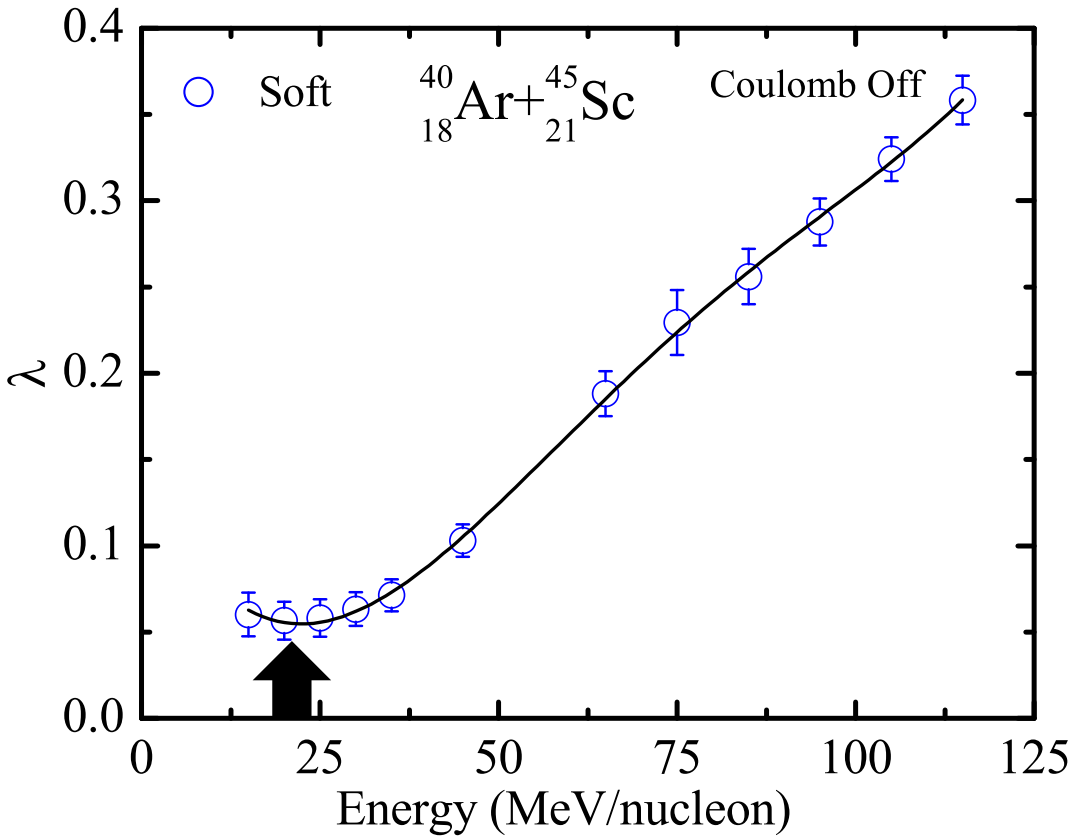


Figure 4.11: Extracted values of parameter $\lambda$ obtained from the exponential fits of intermediate mass fragments as done in Fig. 4.10. Symbols have the same meaning as in Fig. 4.10. Here, solid line represents fourth order polynomial fit of $\lambda$ values obtained using soft equation of state. Solid arrow has same meaning as in Fig. 4.9.

influence of Coulomb forces on the onset of multifragmentation (i.e, critical energy point) for highly charged systems. Therefore, next we will study the isospin effects via Coulomb forces on the onset of multifragmentation in heavily charged system of $^{84}_{36}$Kr + $^{197}_{79}$Au.

### 4.4.2 Onset of multifragmentation in heavily charged system

In Fig. 4.12, we display the charge distributions ($3 \leq Z_f \leq 12$) for highly charged system of $^{84}_{36}$Kr + $^{197}_{79}$Au for six beam energies. The distributions decrease monotonically with increase in the fragment's charge at all incident energies. Here, again power law $\propto Z_f^{-\tau}$ functional form is used to fit the charge distributions and the extracted values of $\tau$ are shown against incident energy in Fig. 4.13. The trends in the displayed values of $\tau$ for both soft and SMD cases are almost in accordance with those observed in Fig. 4.7. The important difference (when compared with Fig. 4.7) that can be seen is that at lower incident energies ($<$ 55 MeV/nucleon), the SMD yields less steeper charge distributions. This may be due to the reason that reaction under consideration is asymmetric and in asymmetric collisions, most of the incident energy is in the form of thermal energy rather than in the form of compressional energy and due to this at lower beam energies, MDIs lead to less compressional zone (due to reduction in the number of binary collisions) and ultimately, give less steeper charge distributions at lower beam energies. Note that extracted values of $\tau$ don't show any critical energy point which may reflect the onset of multifragmentation at beam energies less than 35 MeV/A in the presence of Coulomb forces. To verify this point, we have also performed the calculations in the absence of Coulomb forces for highly charged system and the results for the charge yields and extracted $\tau$ values are plotted in Figs. 4.14 and 4.15, respectively.

In Fig. 4.14, the charge distributions ($3 \leq Z_f \leq 12$) for different incident energies are shown in the absence of Coulomb forces for both soft and SMD cases in the reaction of $^{84}_{36}$Kr + $^{197}_{79}$Au. The extracted $\tau$ values are shown against incident energy in Fig. 4.15. A sharp minimum at an incident energy of $\simeq$ 55 MeV/nucleon is observed both for soft and SMD equations of state, respectively. Again, the charge distributions ($3 \leq Z_f \leq 12$) have been fitted with the exponential fits of the form $\propto e^{-\lambda Z_f}$ for both soft and SMD equations of state in the absence of Coulomb forces (results not shown) and we find that critical energy points using exponential fits are consistent with the ones obtained using power law fits. Comparing with Fig. 4.9, one can see a remarkable effect of the Coulomb forces (due to their long range) for heavily charged system. Also note that for heavily charged

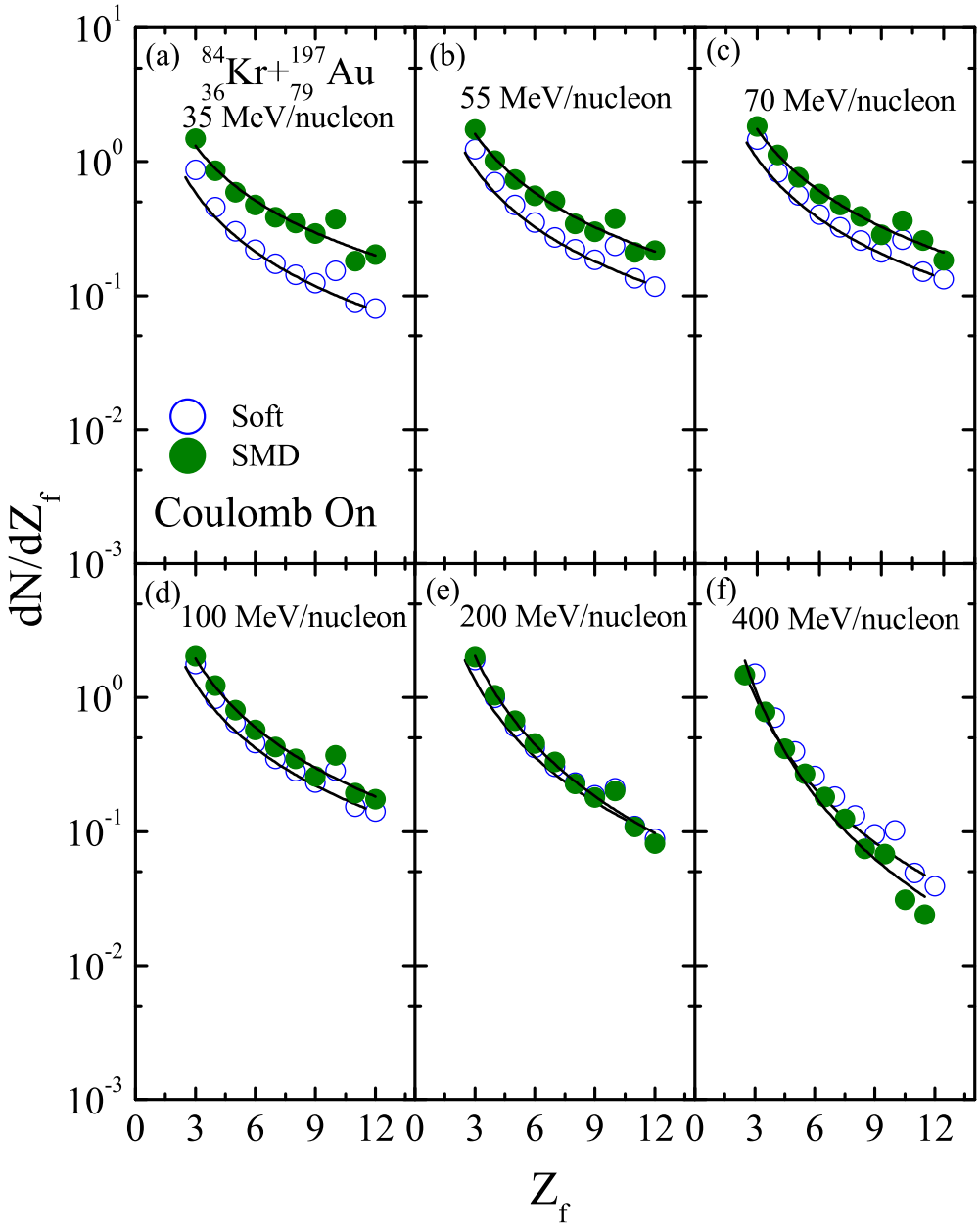


Figure 4.12: The charge distributions obtained for the central collisions of $^{84}_{36}$Kr + $^{197}_{79}$Au at beam energies between 35 and 400 MeV/nucleon for soft and SMD equations of state in the presence of Coulomb forces. Symbols and lines have the same meaning as in Fig. 4.7.

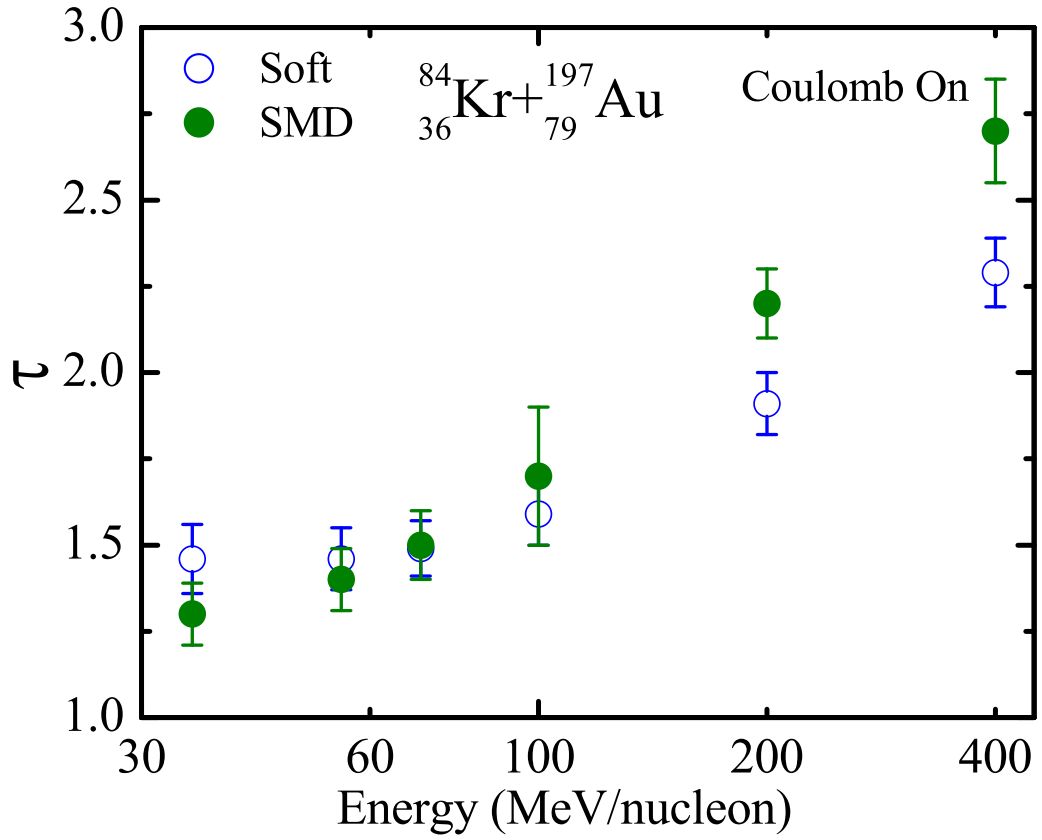


Figure 4.13: Extracted values of parameter $\tau$ obtained from the power law fits of intermediate mass fragments as done in Fig. 4.12 for the central collisions of $^{84}_{36}$Kr + $^{197}_{79}$Au. Symbols have the same meaning as in Fig. 4.12.

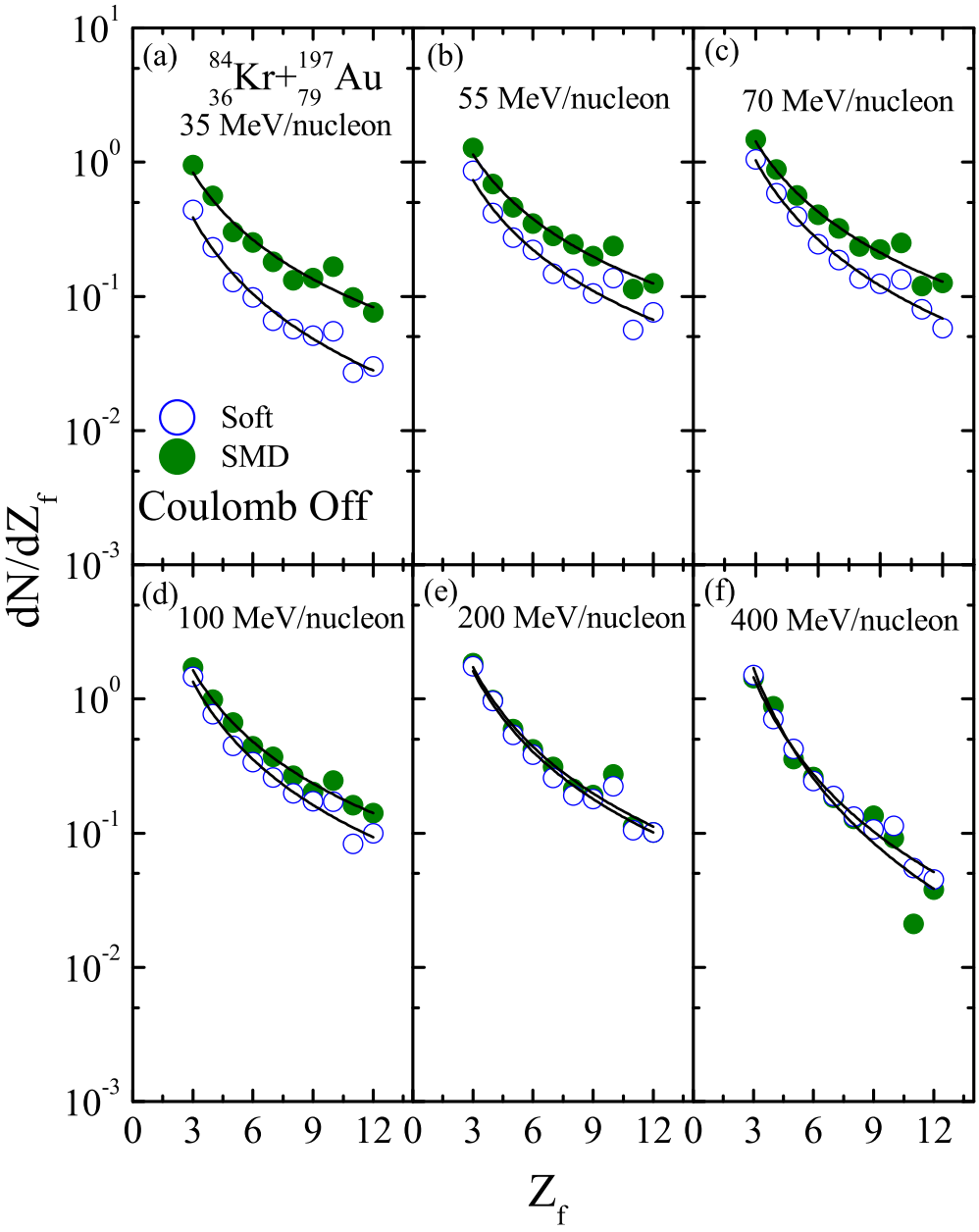


Figure 4.14: Same as Fig. 4.12, but in the absence of Coulomb forces.

system of $^{84}_{36}$Kr + $^{197}_{79}$Au, minimum occurs at higher incident energy when compared with the light charged system of $^{40}_{18}$Ar + $^{45}_{21}$Sc, reflecting the dependence of the critical energy point on the reaction asymmetry as well as on the range of Coulomb forces. On the other hand, total mass of the colliding systems may also shift the onset of multifragmentation. Next, to see the role of momentum-dependent interactions on the critical energy, we do our calculations of $^{40}_{18}$Ar + $^{64}_{29}$Cu (in the absence of Coulomb forces) with soft and SMD equations of state. We find that critical energy is 17 (32) MeV/nucleon with (without) momentum-dependent interactions. The values of $\tau$ for different colliding systems can be summarized in Table 4.2. We clearly see that critical energy increases with system mass, as expected, for both the soft and SMD equations of state. Also, SMD equation of state leads to lower value of the critical energy because of its repulsive nature and the sensitivity of critical energy towards momentum dependence vanishes for heavy systems like $^{84}_{36}$Kr + $^{197}_{79}$Au. From the above discussion and table, we could guess that critical energy for $^{40}_{18}$Ar + $^{45}_{21}$Sc with SMD equation of state should be lower than 17 MeV/nucleon, where IQMD model is not good enough as reported in Ref. [24] and discussed in the Chapter 3. Thus,

Table 4.2: The values of critical energies for three different systems using soft and SMD potentials in the absence of Coulomb forces.

| System | $E^{Critical}_{Soft}$ (MeV/nucleon) | $E^{Critical}_{SMD}$ (MeV/nucleon) |
|---|---|---|
| $^{40}_{18}$Ar + $^{45}_{21}$Sc | 22.07 | not achieved |
| $^{40}_{18}$Ar + $^{64}_{29}$Cu | 32 | 17 |
| $^{84}_{36}$Kr + $^{197}_{79}$Au | 55 | 55 |

from the present calculated results, following broad conclusions can be drawn:

- The onset of multiframentation which may also be related to the nuclear liquid-gas phase transition depends on the incompressibility of nuclear matter;
- The extracted values of $\tau$ can be fitted with fourth order polynomial. The critical energy point occurs at 22.07 ± 0.5 MeV/nucleon when $^{40}_{18}$Ar + $^{45}_{21}$Sc reaction is simulated using soft equation of state without Coulomb potential. This critical energy is consistent with the one reported in Ref. [121] for the same system and;
- Calculations performed in the absence of Coulomb forces lead to minimum in the

extracted $\tau$ values, which in turn, becomes more sharp for heavily charged system of $^{84}_{36}$Kr + $^{197}_{79}$Au.

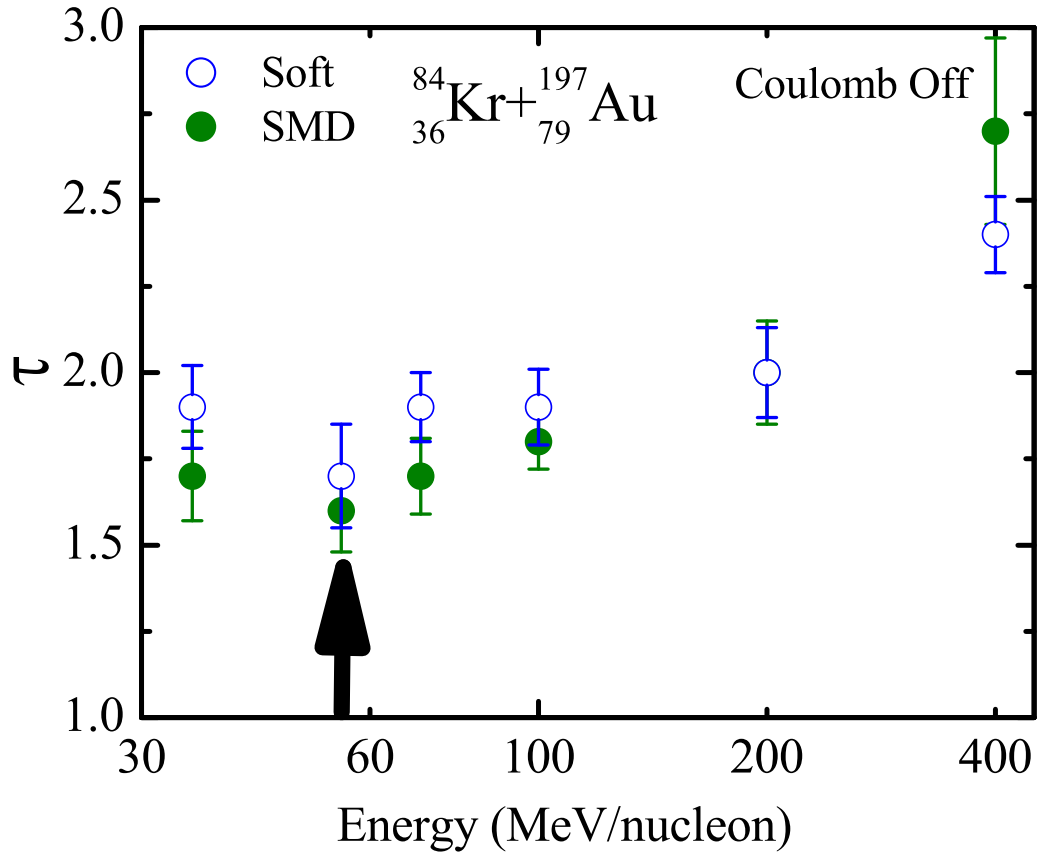


Figure 4.15: Same as Fig. 4.13, but in the absence of Coulomb forces. Here, solid arrow corresponds to the sharp minimum in the extracted values of $\tau$ for soft and SMD equations of state.

## 4.5 Comparison with experimental data

Further, we confront our theoretical calculations using the IQMD model with experimental measurements of INDRA collaboration [314, 315] to present the suitability (to explain the measured charge yield of IMFs in the range $3 \leq Z_f \leq 12$ at low incident energies; as this range of IMFs is used to predict the onset of multiframentation i.e., liquid-gas phase transition in nuclear matter) of theoretical approach used in the present study.

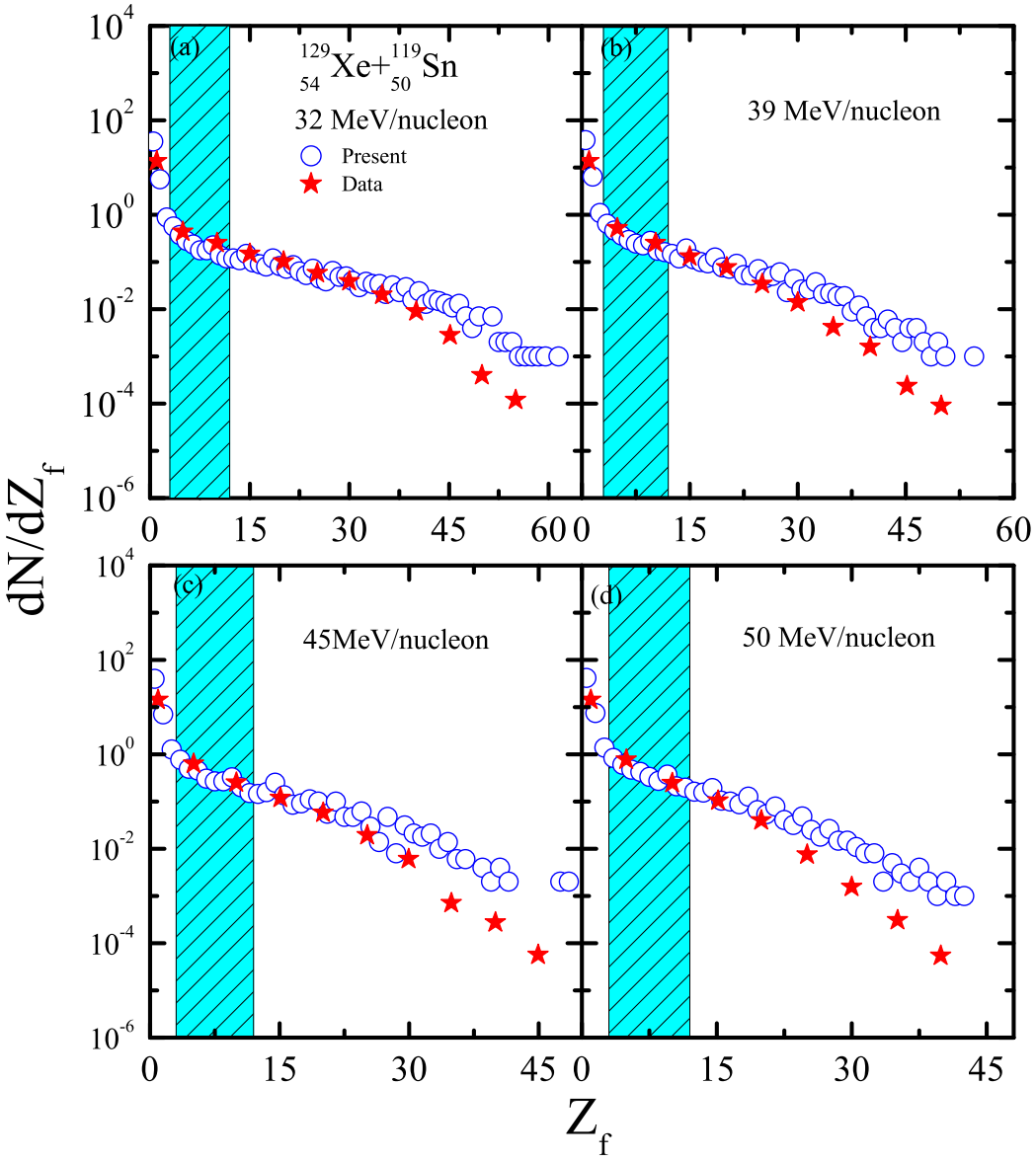


Figure 4.16: The charge distributions for the central collisions of $^{129}_{54}$Xe + $^{119}_{50}$Sn at beam energies of 32, 39, 45 and 50 MeV/nucleon. Open circles represent our present calculations and stars correspond to experimental data of source Ref. [314] and extracted from Ref. [316]. The shaded region represents the yield of intermediate mass fragments in the range $3 \leq Z_f \leq 12$; which is taken into consideration for the calculations regarding the onset of multifragmentation.

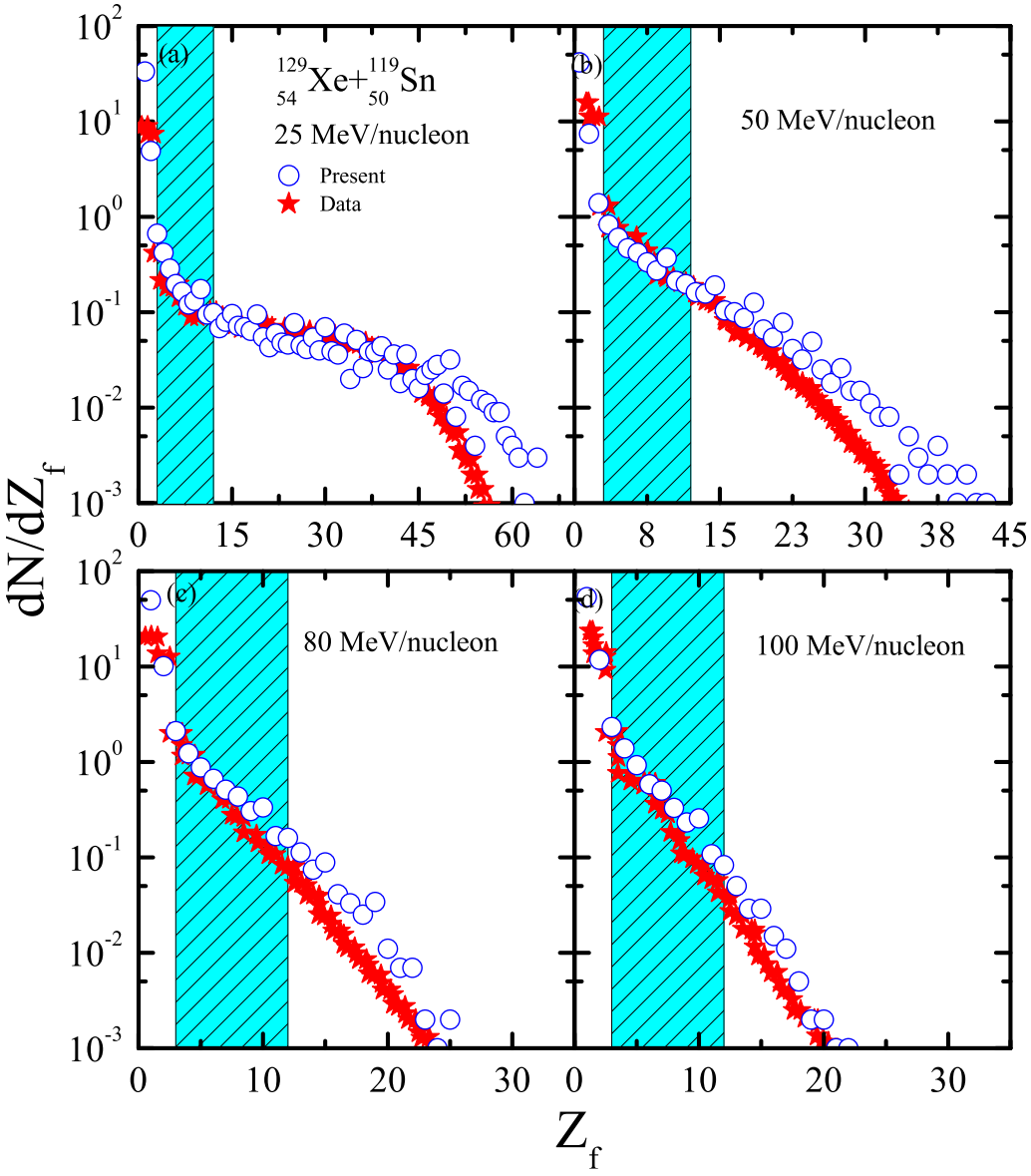


Figure 4.17: Same as Fig. 4.16, but at beam energies of 25, 50, 80 and 100 MeV/nucleon. Here, the experimental data is extracted from Ref. [315].

Note that recently [24] (also stated in the Chapter 3), we have made an extensive study of the fragmentation pattern for various asymmetric reactions using isospin-dependent quantum molecular dynamics model and confront our theoretical calculations with the available experimental data as well as various other model results and our detailed analysis revealed that isospin-dependent quantum molecular dynamics model calculations nicely reproduce the measurements of asymmetric reactions around Fermi-energies. In Fig. 4.16, we display the charge distributions for nearly symmetric reactions of $^{129}_{54}$Xe + $^{119}_{50}$Sn at different bombarding energies of E = 32, 39, 45 and 50 MeV/nucleon. Open circles represent our theoretical calculations and stars show the experimental data taken from source Ref. [314] and extracted from Ref. [316]. We find reasonably good agreement of our model results with the measured charge distributions. It is worth mentioning that our present aim is to concentrate on the yield of intermediate mass fragments which lie in the range $3 \leq Z_f \leq 12$ to extract the critical exponents as well as critical energy and the yield of fragments in the above said charge range is in nice agreement with measured yield (see shaded region).

Next, we also compare our IQMD model results with the experimental measurements of Ref. [315] where reactions of $^{129}_{54}$Xe + $^{119}_{50}$Sn have been studied at 25, 80 and 100 MeV/nucleon also and results are shown in Fig. 4.17. The symbols have the same meaning as reported in previous figures. Again we find that our calculated results for the yield of fragments (which lie in the range ($3 \leq Z_f \leq 12$)) are in nice agreement with measured ones. Therefore, the last two figures of this chapter made the present approach (i.e., IQMD model) more reliable in explaining the critical exponents (first order liquid-gas phase transition in the nuclear matter) at intermediate energy heavy-ion collisions.

## 4.6 Summary

We studied the isospin effects via Coulomb forces on the charge distributions and on the onset of multifragmentation in light and heavily charged systems using soft and soft with momentum-dependent interactions. Our study met with the conclusion that Coulomb forces affect the critical energy point both in light and heavily charged systems and resulted in the shift of the critical energy point to lower (higher) incident energy value in the presence (absence) of Coulomb forces. Also, the onset of multifragmentation depends on the reaction asymmetry as well on the strength of the Coulomb forces as

critical energy point is more sharp for heavily charged system of $^{84}_{36}$Kr + $^{197}_{79}$Au when compared with the light charged system of $^{40}_{18}$Ar + $^{45}_{21}$Sc where a small dip has been observed.